

Distribution dynamics of fisher and Wigner–Yanase information correlations of two qubits coupled to an open superconducting cavity

F. M. Aldosari , A.-B. A. Mohamed *, A. Rahman † and M. Hashem ‡

**Department of Mathematics, College of Science and Humanities in Al-Aflaj,
Prince Sattam bin Abdulaziz University, Saudi Arabia*

†*School of Physics, University of Chinese Academy of Science,
Yuquan Road 19A, Beijing 100049, P. R. China*

‡*Department of Mathematics, Faculty of Science,
Assiut University, Assiut, Egypt*
 abdelbastm@aun.edu.eg

Received 21 March 2023

Revised 25 September 2023

Accepted 27 September 2023

Published 4 November 2023

In this paper, we explore distribution dynamics of two-qubit Fisher and skew information correlations of a dissipative microwave cavity field interacting with two charged superconducting qubits. Besides the negativity function, non-classical correlations beyond entanglement are studied using local quantum Fisher information (LQFI) and local quantum uncertainty (LQU). We find that the two-qubit non-classical correlations are sensitive to qubit–qubit distribution angle, two-qubit dissipation parameter, and initial coherent state intensity. The phenomena of frozen quantum correlations, sudden death or birth, as well as revival dynamical maps are feasible in the current two-qubit state when exposed to a microwave cavity. The non-classical correlations and entanglement have been found damped under the two-qubit dissipation appearance in the field. For the increasing strength of coherence intensity of the field, the two-qubit non-classical correlations functions remain to emerge quickly and oscillate with higher frequency, although with the least amplitudes. Interestingly, unlike the non-classical correlations, negativity does not emerge against higher coherence strengths of the cavity and remains completely zero. Finally, for the least dissipation and higher coherence strength, one can readily generate non-classical two-qubit states employing a microwave cavity.

Keywords: Local Fisher information; local quantum uncertainty; dissipation.

PACS Nos.: 03.67.-a, 03.67.Mn, 03.67.Pp

^{*}Corresponding author.

1. Introduction

Non-classical correlations are the main subject of concern in the developing discipline of quantum information theory.¹ A key feature of quantum particles is quantum entanglement, which is a particular kind of non-classical correlation among quantum entities.² Besides, quantum entanglement is known to be the key distinction between quantum and classical correlations, and by any means, it cannot be observed in classical objects. Quantum entanglement has been shown by recent tests in many-body optical lattice systems.³ Certain applications, such as quantum teleportation,⁴ cryptography,⁵ key-distribution,⁶ dense coding,⁷ and microscopy⁸ are highly based on entanglement. Therefore, in the past decade, entanglement has become the prime topic of investigation for quantum researchers.^{9,10} There exist other types of non-classical correlations beyond quantum entanglement that offer specific traits as resources for quantum mechanical protocols.¹¹ These non-classical correlations include measurement-induced disturbance,¹² measurement-induced non-locality,^{13,14} quantum discord,^{15,16} and geometric quantum discord.¹⁷ In the current case, besides investigating negativity entanglement, we focus on some advanced quantum correlation functions known as local quantum Fisher information (LQFI)^{18–21} and local quantum uncertainty (LQU).^{22–24} Investigating such non-classical correlations may enable us to know how much they are strengthened compared to the entanglement or how much they emerge or decay with time in quantum systems.

The appropriate characterization of non-classical correlations in the quantum systems may lead to leading-edge quantum memories which may have optimal characteristics of preservation properties. By using various measuring techniques to find the degree of quantum correlations between the sub-systems of a composite state, this problem can be solved. Girolami *et al.* have proposed LQU as a discord-like indicator of non-classical correlation.²³ LQU measure uses the concept of Wigner-Yanase skew information where minimum uncertainty is induced by applying local measurements on a single sub-system of a composite state.²⁵ This indicator satisfies all the requirements of a reliable quantum correlation measure and can be linked to quantum Fisher information (QFI). Using the concept of QFI, to determine the degree of non-classical correlations, the notion of LQFI has been introduced.²² It has already been established that the skew information is majorized by the unitary evolution of a density matrix as measured by the QFI measurement concerning the phase parameter. This measure is established using optimization techniques over the observables related to one of the sub-components. Additionally, to improve the accuracy and efficiency of quantum metrology operations, LQFI provides a way to understand how quantum correlations function.

The tremendous increase in demand for superconducting microwave cavities over the last 10 years has been driven mostly by the growing importance of quantum computing using artificial atoms.^{26,27} Nevertheless, these devices' capabilities are not only constrained to quantum information and computing protocols. For instance, for squeezed microwave fields in quantum optics, by flux-tuning, these resources are

used in a superconducting quantum interference device, which amplifies quantum fluctuations in superconducting cavities.²⁸ Besides, superconducting cavities can be practically designed by establishing a Josephson connection or a superconducting tunnel junction between a small superconducting island and a nearby superconducting reservoir.^{29,30} The number of Cooper pairs transported across the junction determines the cavity's state. Such an “island’s” charge states contain extra electrons than the charge states of an ion, which may be an atom or molecule.^{31,32} By projecting charge states and employing the voltage output that controls the chemical potential of the island, coherence and entanglement can be achieved.³³ To reach quantum supremacy, there has been an increasing push to create quite powerful and dependable quantum computers in current history.^{34,35} Because of the generality and success academics have had in developing a technique for quantum logic circuits, superconducting qubits have been among the most widely used realistic insights of quantum computing.³⁶

In this work, we consider the dynamics of two superconducting charge qubits coupled with a microwave cavity. In particular, special emphasis on the dynamics of entanglement, and non-classical correlations, such as LQU and LQFI is made. Designing efficient quantum mechanical protocols, devices, transmitting channels and memories remains a hotly debated topic among quantum computing researchers, and in particular, the preservation of quantum correlations is the main concern for them. This is done by employing several types of protocols, channels, and memories, however, there is still room for improvement. For example, in Refs. 37–40, several types of classical channels have been employed for the dynamics of open biqudit, triqubit, and multiqubit states for quantum information processing, however, the processes have been found highly degrading. The entanglement and coherence generation has been found depending on the two-exciton decay, and the initial coupling intensity of the coherence of microcavity, however, with regions where quantum correlations become completely vanished.³⁹ Motivated by these studies, we aim to investigate the state dependence on various associated parameters such as coherent state intensity, two-qubit dissipation rate, and the linking strength between the qubits and cavity. Besides, the case of controlling the qubit-cavity interaction is realized by tuning the gate voltage and associated magnetic field.⁴¹ In the case of quantum correlations generation, other studies have also been presented which disclose the significance of various techniques, parameterization, phenomena, fields, and configurations.^{42–48}

This paper is structured as follows. In Sec. 2, we discuss the physical model of the current assumed system. Section 3 describes the computation of non-classical correlations functions while Sec. 4 presents the obtained results and discussion. In Sec. 5, we will finally summarize our results.

2. Driven Two Charge-Qubits Superconducting (SC) Model

The considered model describes two charge SC-qubits strongly (each one has the charging energy E_C) coupled to an SC-cavity through two Cooper pair boxes (CPB),

each CPB is coupled to a gate voltage V_g , gate capacitor C_g , and dimensionless gate charge $n_g = \frac{C_g V_g}{2e}$. The CPB contains a small SC-island and two Josephson junctions (they have the same Josephson energy E_J and capacitance C_J).^{49,50} The microwave SC-cavity field is described by creation \hat{a}^\dagger and annihilation \hat{a} operators with the frequency ω . Each charge-qubit has up $|1\rangle_i$ and lower $|0\rangle_i$ charge states and is described by Pauli matrices $\hat{\sigma}_\pm^i$. To complete dispersive two-qubit system engineering, the magnetic flux ϕ_c and the flux quantum of the applied classical magnetic field satisfy $\phi_c = \frac{1}{2}\phi_0$ and $n_g \neq \frac{1}{2}$. After considering the dispersive regime (or with large detuning $\delta = 2E_C - \omega = \frac{2e^2(2n_g-1)}{(C_g+2C_J)} - \omega$), the dispersive SC qubit-cavity interaction Hamiltonian is given by Ref. 50

$$\hat{H}_{\text{dis}} = \sum_{i=A,B} \lambda \{ \hat{\sigma}_+^i \hat{\sigma}_-^i \hat{a} \hat{a}^\dagger - \hat{\sigma}_-^i \hat{\sigma}_+^i \hat{a}^\dagger \hat{a} + \hat{\sigma}_+^A \otimes \hat{\sigma}_-^B + \hat{\sigma}_-^A \otimes \hat{\sigma}_+^B \}. \quad (1)$$

The dispersive qubit-cavity coupling is described by $\lambda = \frac{\pi^2 |\eta_i|^2 E_J^2}{\delta \phi_0^2}$, and depends on the physical properties of charge qubits while the parameters $\eta_i (i = A, B)$ depend on the properties of the SC-cavity and the Cooper pair boxes, and it has a unit of magnetic flux.

At zero temperature, the master equation that describes the time-dependent of the dissipative qubit-cavity state, $\hat{M}(t)$, is given by

$$\frac{d}{dt} \hat{M}(t) = i[\hat{M}, \hat{H}_{\text{dis}}] + \mathcal{L}_Q \hat{M} + \mathcal{L}_C \hat{M} + \mathcal{L}_{\text{Phase}} \hat{M}. \quad (2)$$

The \mathcal{L}_Q and \mathcal{L}_C , respectively, describe two-qubit decay (with spontaneous-emission rates γ_{Q_k} , $k = A, B$) that is due to background modes other than the privileged cavity field, and cavity-field damping (with cavity decay constant γ_C) that is due to the standard vacuum reservoir. While $\mathcal{L}_{\text{Phase}}$ describes a dephasing of the qubit/cavity coherence. To explore distribution dynamics of the two-qubit Fisher and skew information correlations under the two-qubit spontaneous decay, we consider only the two-qubit dissipation induced by the spontaneous-emission decay. Therefore, the considered master equation describes only the two-qubit dissipation

$$\frac{d}{dt} \hat{M}(t) = i[\hat{M}, \hat{H}_{\text{dis}}] + \sum_{k=A,B} \gamma_{Q_k} [2|0_k\rangle\langle 1_k| \hat{M} |1_k\rangle\langle 0_k| - |1_k\rangle\langle 1_k| \hat{M} - \hat{M} |1_k\rangle\langle 1_k|]. \quad (3)$$

We consider $\gamma_{Q_k} = \gamma$ and the SC-cavity field starts with a coherent state

$$|\xi\rangle = \sum_{n=0}^{\infty} \frac{\xi^n e^{-\frac{1}{2}|\xi|^2}}{\sqrt{n!}} |n\rangle, \quad (4)$$

where ξ is the initial coherent amplitude and $|\xi|^2$ is the initial coherent intensity. While the two charge-qubit state starts a superposition of their up and lower states, i.e. $M^{AB}(0) = |\phi\rangle\langle\phi|$, where $|\phi\rangle = (\sin\phi|1_A\rangle + \cos\phi|0_A\rangle)(\sin\phi|1_B\rangle + \cos\phi|0_B\rangle)$.

In the two charge-qubits state bases: $\{|\varpi_1\rangle = |1_A 1_B\rangle, |\varpi_2\rangle = |1_A 0_B\rangle, |\varpi_3\rangle = |0_A 1_B\rangle, |\varpi_4\rangle = |0_A 0_B\rangle\}$, the two-charge-qubit density matrix is given by

$$M^{AB}(t) = \sum_{i=1}^4 \sum_{j=1}^4 m_{ij} |\varpi_i\rangle \langle \varpi_j|, \quad (5)$$

m_{ij} ($i, j = 1 - 4$) are given by

$$\begin{aligned} m_{11} &= e^{-4\gamma t} \sin^4 \phi, \\ m_{12} = m_{13} = m_{21}^* = m_{31}^* &= e^{-|\xi|^2(1-e^{-2i\lambda t})-3\gamma t} \sin^3 \phi \cos \phi, \\ m_{14} = m_{41}^* &= e^{-2i\lambda t-|\xi|^2(1-e^{-4i\lambda t})-2\gamma t} \sin^2 \phi \cos^2 \phi, \\ m_{22} &= e^{-2\gamma t} \cos^2 \phi \sin^2 \phi + (1 - e^{-2\gamma t}) e^{-2\gamma t} \sin^4 \phi, \\ m_{23} = m_{23}^* &= e^{-2\gamma t} \sin \phi \cos \phi, \\ m_{24} = m_{42}^* &= \frac{1}{2} e^{-|\xi|^2(1-e^{-2i\lambda t})-\gamma t} \left[\frac{\gamma \sin^2 \phi \sin 2\phi}{i\lambda - \gamma} (e^{-2\gamma t} - e^{-2i\lambda t}) + \sin \phi \cos^2 \phi \right], \\ m_{34} = m_{43}^* &= -\frac{1}{2} e^{-|\xi|^2(1-e^{-2i\lambda t})-\gamma t} \left[\frac{\gamma \sin^2 \phi \sin 2\phi}{i\lambda - \gamma} (e^{-2\gamma t} - e^{-2i\lambda t}) + \sin \phi \cos^2 \phi \right], \\ m_{44} &= (e^{-2\gamma t} - 1)^2 \sin^4 \phi - 2(e^{-2\gamma t} - 1) \sin^2 \phi \cos^2 \phi + \cos^4 \phi. \end{aligned}$$

The general two charge-qubit state $M^{AB}(t)$ is used to explore some dynamical properties of two-qubit distribution Fisher and skew information correlations.

3. Fisher and Skew Information Correlation Quantifiers

3.1. Local quantum-fisher information (LQFI)

Here, we use LQFI as a good measure for generating two-charge-qubits non-classical correlations. For the general two charge-qubit state $M^{AB}(t)$ that can be rewritten as $M^{AB} = \sum_m E_m |E_m\rangle \langle E_m|$ with $E_m \geq 0$ and $\sum_m E_m = 1$, the closed expression of the LQFI is given by^{18,19}

$$F(t) = 1 - \pi_W^{\max}, \quad (6)$$

where π_W^{\max} is the highest eigenvalue of the symmetric matrix $W = [w_{ij}]$ ($ij = x, y, z$), where

$$w_{ij} = \sum_{m,n} \frac{2E_m E_n}{E_m + E_n} \mathcal{R}_{mn}^i \mathcal{R}_{nm}^{i\dagger}, \quad \mathcal{R}_{mn}^i = \langle E_m | I_A \otimes \sigma_{A/B}^i | E_n \rangle.$$

3.2. Local quantum uncertainty LQU

The LQU^{23,51} is used to measure the maximal nonlocal correlation of the Wigner–Yanase skew information. For the general two charge-qubits state $M^{AB}(t)$, the LQU reduces to be²³

$$L(t) = 1 - \lambda_{\max}(Y_{AB}), \quad (7)$$

where $\lambda_{\max}(.)$ is the largest eigenvalue of the matrix $Y = [y_{ij}]$ ($ij = 1, 2, 3$)

$$y_{ij} = \text{Tr} \left\{ \sqrt{M^{AB}(t)} (\sigma^i \otimes I) \sqrt{M^{AB}(t)} (\sigma^j \otimes I) \right\} \quad (8)$$

and σ^i are Pauli operators.

3.3. Negativity entanglement

For the general two charge-qubit state $M^{AB}(t)$, the negativity is defined by Ref. 52

$$N(t) = 2 \sum_i |\mu_i|, \quad (9)$$

where μ_i are the negative eigenvalues of the resulted matrix after making partial transpose for the general two charge-qubits state $M^{AB}(t)$ with respect to A/B -qubit. The two-charge-qubits negativity $N(t)$ has a zero value for the uncorrelated two-charge-qubits state. Otherwise, it satisfies $0 < N(t) < 1$ for the correlated two-charge-qubit state.

4. Computational Results

In this section, we examine the results obtained using the final density matrix for the general two charge-qubit state $M^{AB}(t)$ coupled with an external microwave cavity under the two-qubit dissipation effects. Next, we have done computing the non-classical correlations in the state using LQFI and LQU given in Eqs. (6) and (8). Besides this, we computed entanglement using the negativity function given in Eq. (9). In the current case study, we aim to provide a detailed analysis of the dynamics of quantum correlations generation, preservation, and decay. For this reason, we use different parameter ranges such that to examine the associated impact when they are set to weak as well as strong strengths. Figure 1 displays the effect of the distribution angle of the initial two-qubit state ϕ on the quantum correlations measures LQFI, LQU, and negativity for $\phi \in [0, \pi]$ in the absence of the two-qubit dissipation parameter $\gamma = 0$ while setting the coherent intensity to unity. Initially, the LQFI, LQU, and negativity functions remain completely zero, suggesting that the system is in its full product state form with no quantum correlations. With time, and for the increasing coupling strength λt (the dispersive qubit-cavity coupling λ depends on the physical properties of the charge qubits), the non-classical correlations functions LQFI (Fig. 1(a)) and LQU (Fig. 1(b)) get generated which can be traced back to Ref. 53. Likewise, in Fig. 1(c), the negativity function also gets induced and increases with time, therefore suggesting the generation of quantum correlations and entanglement in the state. However, the generation map of the non-classical correlations remains quite different. For example, the quantum correlations function LQFI and LQU reach their first maximum quickly and then oscillate for some interval at the highest level. However, the negativity function reaches smoothly to its maximum without showing any revivals at its highest level. Both the LQFI and

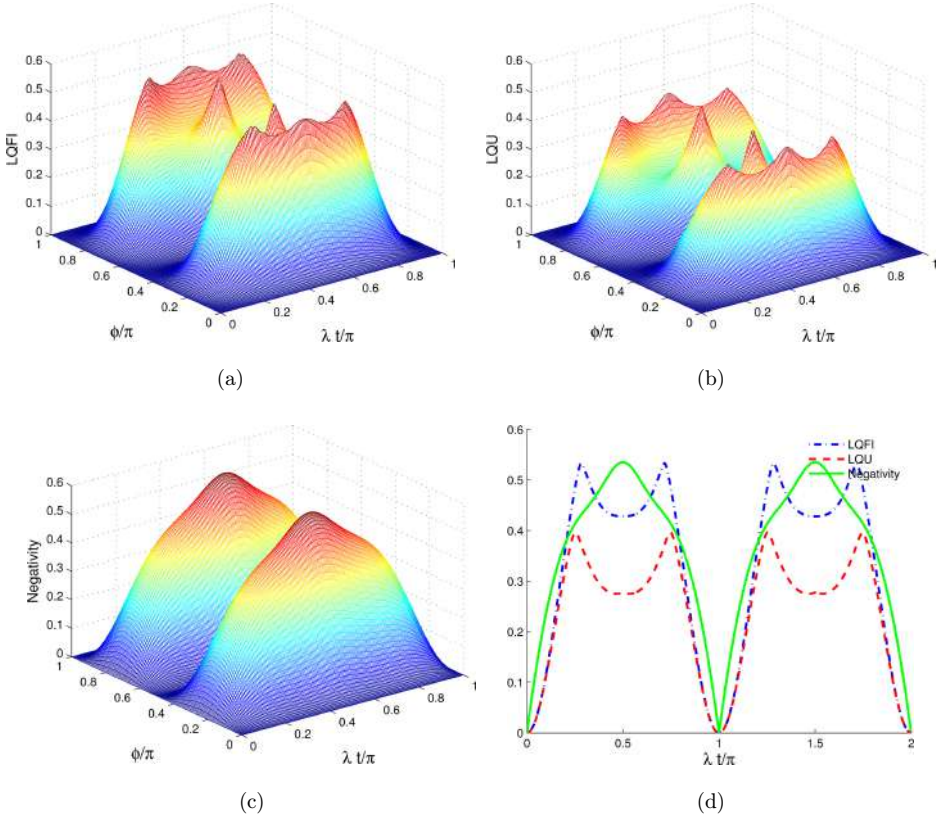


Fig. 1. The dynamics of (a) two-qubit LQFI, (b) LQU, and (c) $N(t)$ for the angle $\phi \in [0, \pi]$, $\xi = 1$ and $\gamma = 0$ against the time. (d) The dynamics of two-qubit LQFI, LQU, and $N(t)$ distribution intersection for $\phi = 0.2\pi$, $\xi = 1$, and $\gamma = 0$.

LQU functions, nonetheless, strictly agree with each other qualitatively. In quantitative terms, the LQFI function reaches a higher level than the LQU function, i.e. meaning that the prior function captures a greater amount of quantum correlations than the latter one. After a specific coupling time, the LQFI and LQU correlations and entanglement functions get reduced and finally achieve zero saturation level. Hence, the existence of LQFI and LQU correlations and entanglement can only be observed in the state for a certain range of interaction strength and time. Besides this, the LQFI and LQU correlations and entanglement emergence and decay into the state seem completely dependent upon certain values of ϕ . As there is a certain region in the state's space where the LQFI and LQU correlations functions, LQFI and LQU as well as entanglement function negativity completely agree. Furthermore, there are also regions of ϕ where the non-classical correlations and negativity functions get maximum, for instance, see at $\phi \approx [0.2, 0.8]$. The sudden death and birth transitions of

non-classical correlations and entanglement in the state, therefore, both are dependent upon the different values of λt and ϕ . In Fig. 1(d), we evidence the similar dynamical maps for LQFI, LQU, and negativity as depicted in Figs. 1(a)–1(c). As can be seen, in both cases (3D and 2D graphs), the initial, as well as the final values of non-classical correlations and entanglement remain the same. Besides, the transitions of the state between product state and resource state occur approximately at the comparable time. Hence, there is a strong consistency between them.

Figure 2 shows the joint effect of coupling strength λt and two-qubit dissipation parameter γ/λ on the dynamics of LQFI, LQU, and negativity in a two-qubit state. Unlike the case in Fig. 1 ($\gamma = 0$), we have raised the two-qubit dissipation rate and is set as $0 \leq \gamma/\lambda \leq 0.5$ in Figs. 2(a)–2(c). This leads to change in the dynamical map of the two-qubit system and associated quantum correlations at intervals. Initially, the state remains completely separable, as negativity and non-classical correlations function LQFI and LQU start from zero. With time, these functions growth to their maximum, ensuring the emergence of quantum correlations (Figs. 2(a) and 2(b))

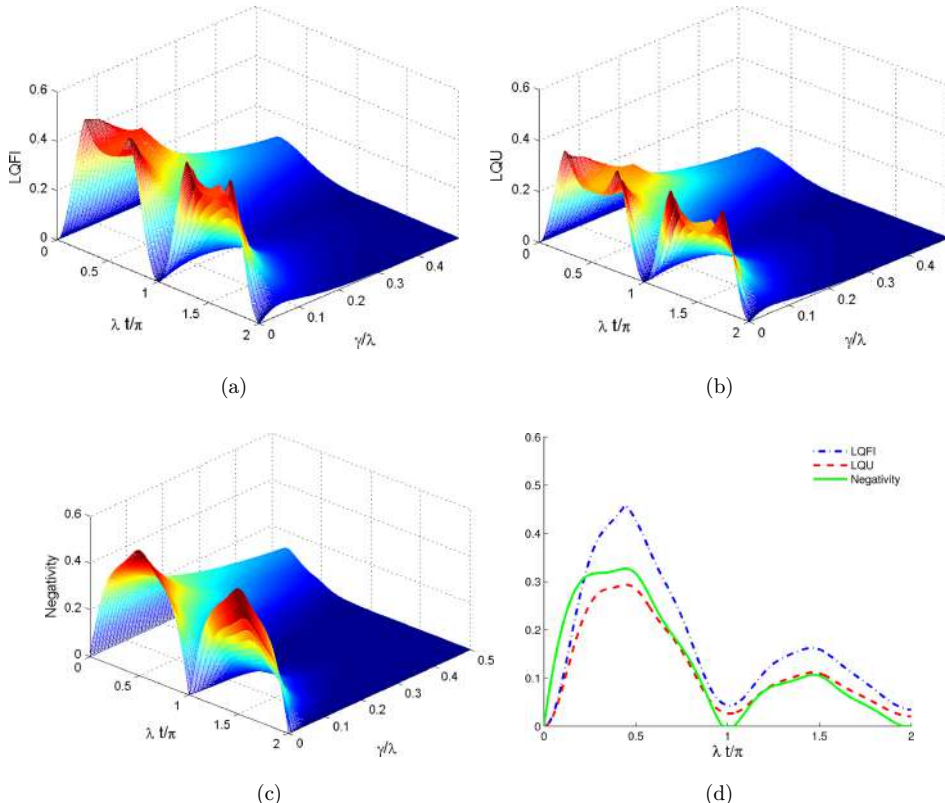


Fig. 2. Non-classical correlations under the two-qubit dissipation, $\gamma \in [0, 0.5\lambda]$. (d) displays NCs for $\phi = 0.2\pi$, $\gamma = 0.1\lambda$ and $\xi = 1$.

and entanglement (Fig. 2(c)) in the state. However, the impact of increasing values of the λ and γ on the behavioral dynamics of quantum correlations remained completely different from each other. Except at the coupling interaction strength time $\lambda t \in [0, 1, 2]$, the state remains entangled and quantum correlated. However, for the increasing strength of the two-qubit dissipation γ , the negativity as well as the LQFI and LQU functions remained largely suppressed. Besides, for the lower interaction strength and time, the damping of the negativity is small, for example, see the region $0 \leq \lambda t \leq 1$. Nonetheless, the damping increases as the coupling strength with time increases, for example, in the region $1 \leq \lambda t \leq 2$. Besides, in Fig. 2(d), the simultaneous dynamics of LQFI, LQU, and negativity in a two-qubit state are discussed but for $\gamma = 0.1\lambda$. The initial level of non-classical correlations and entanglement functions remains zero in Fig. 2(d) and agrees with that in Figs. 2(a)–2(c). However, the final levels of LQFI, LQU, and negativity do not meet with that encountered in Figs. 2(a)–2(c) for the higher values of γ . As in Figs. 2(a)–2(c), the quantum correlations and entanglement remained suppressed against the higher values of the parameter γ at the final notes of interaction time. On the contrary, the LQFI, LQU, and negativity

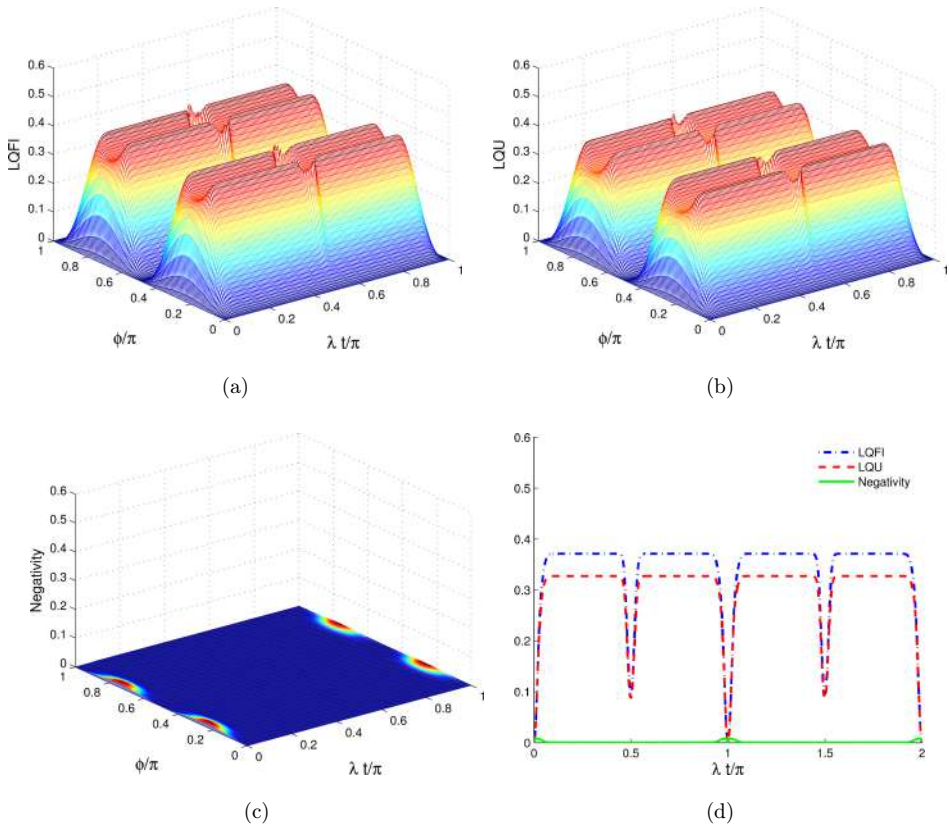


Fig. 3. Dynamics of LQFI, LQU, and negativity of Fig. 1 but for $\xi = 5$.

remain nonzero, even at the given final notes of interaction time. Therefore, the assumed two-qubit quantum correlations remain fragile against the higher two-qubit dissipation rate of the microwave cavity.

In Fig. 3, we investigate the joint impact of ϕ and γ under the increased coherence strength ξ of the cavity on the dynamics of LQFI, LQU, and negativity in a two-qubit state coupled with a microwave cavity. The time dynamical map of the non-classical correlations and entanglement in the system becomes different from that found in Figs. 1 and 2, although, we have repeated the parameter configuration, except, setting $\xi = 5$ instead of $\xi = 1$. At the onset, the state remained completely separable and local, which agrees with the results in Figs. 1 and 2. As the interaction between the microwave cavity and state is further increased, the non-classical correlations in the state appear. The speed of emergence of the non-classical correlations (Figs. 3(a) and 3(b)) in the current case is enough higher than that found in Figs. 1 and 2. This means that increasing the coherence strength of the microwave cavity can speed up the process of generating quantum correlations in completely separable states. The generation of non-classical correlations in the two-particle classical state both remained dependent upon the coupling strength λt and parameter ϕ of the state. In particular, the existence of non-classical correlations depends upon specific values of λ and ϕ . For instance, $\phi \in [0, 0.5, 1]$ should be avoided where the state becomes completely separable. Besides, at $\lambda t = 0.5$, there is a small decline of quantum correlations, however, they do not undergo complete death. Interestingly, the negativity function (Fig. 3(c)) shows no rise against the current parameter setting of the cavity, hence, strongly contradicting the results of LQFI and LQU. In Fig. 3(d), the two-dimensional dynamics of the non-classical correlations and entanglement against coupling strength and interaction time λt is studied. The results well agree with those obtained in Figs. 3(a)-3(c), except for the point that there exist sudden deaths of LQFI and LQU correlations periodically against λt . Besides, there is a tiny emerging region of negativity at places where LQFI and LQU functions become zero. This is quite unusual in the current case, as generally, all types of quantum correlation are directly dependent upon each other. This fact states that the current parametrization of the field acts differently towards entanglement and other non-classical correlations, such as LQFI and LQU.

In Fig. 4, the impact of different coherence intensity strengths of the microwave cavity on the dynamics and generation of LQFI and LQU correlations and entanglement in the two-qubit state is analyzed. In agreement with Figs. 1–3, the state remained fully separable initially. However, for the increasing interaction time and strength of the field, the LQFI and LQU remain increasing functions of non-classical correlations in time (Figs. 3(a) and 3(b)). On the contrary, the negativity function in Fig. 4(a) rises to a smaller level and then drops, remaining mostly zero compared to the LQFI and LQU when $\xi = 2$. On the other hand, the entanglement function remains completely zero in Fig. 4(b) for higher coherence strengths $\xi = 5$. Hence, this suggests that entanglement cannot nourish in the two-qubit state when coupled with the highly coherent conditions of the microwave cavity. Besides, for the increasing

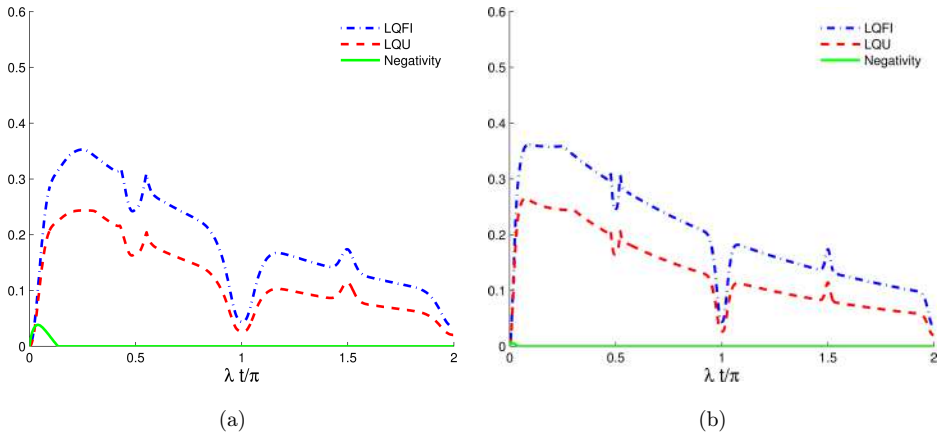


Fig. 4. Dynamics of LQFI, LQU, and negativity is displayed with $\phi = 0.2\pi$ and $\gamma = 0.1\lambda$ for different values of ξ : $\xi = 2$ in (a) and $\xi = 5$ in (b).

interaction strength and time, the LQFI and LQU correlations functions get developed quickly, but, then evolve with damping amplitudes. It seems that after some given time, the LQFI and LQU will freeze. Comparatively, the non-classical correlations in the two-qubit state generate at a higher speed against the higher strengths of coherence intensity $\xi = 5$ (Fig. 4(b)). While for the low ξ values, the generating speed of quantum correlations remained slower as obtained in Fig. 4(a). Hence, suggesting the supportive nature of the coherence intensity towards LQFI and LQU functions.

In Figs. 3 and 4, we illustrated in detail the generation of quantum correlation against varying coherence intensity strengths of the cavity. It turns out true that the increasing strength of coherence of the cavity impact positively the generation of quantum correlations. Not only the rate of generation but the pattern of dynamical maps also changes with changing the strength of the cavity coherence state. For example, for the increased coherence strengths, the generation of quantum correlations takes place at a high speed (see Fig. 4(a)) and so the opposite (Fig. 4(b)). Besides, it is interesting to note that the increased coherence strengths impact differently the generation of different types of non-classical correlations. For example, for the increased coherence strengths, the rate of generation of LQFI, LQU, and negativity remains different, see Figs. 3(a)–3(c). Negativity is highly suppressed by the increased coherence strength compared to the LQFI and LQU measures.

In this study, the LQFI is witnessed to achieve higher maximums than the relative LQU and negativity functions. This suggests that the non-classical correlations shown by LQFI remained more efficient, and emerged quickly to a higher degree in the current two-qubit state. Besides, we find that the non-classical correlations and entanglement functions suffer sudden deaths and births. However, note that we have considered a completely separable and non-correlated state. This means that the current microwave cavity remains a vital resource for the generation of LQFI and

LQU correlations in quantum systems. The sudden deaths and births or revivals in LQFI and LQU correlations and entanglement functions suggest successful information and attribute exchange between the microwave cavity and state. This also can be interpreted as the successful transformation of the classical product states into resourceful nonlocal states. This behavior of the microwave cavity towards the generation and dynamics of the biqudit quantum correlations contradicts the role of the Fock state cavity field.^{53–55} In the case of quantum channels with memory, at certain values of the relative parameters of channels, quantum correlations can be kept preserved, however, the generation of quantum correlations is still not feasible through them.⁵⁶ Similarly, the correlated nonlocal dephasing channels have been shown to have the least possible losses but the generation of quantum correlations in the two-qubit state is not feasible.⁵⁷ Hence, the current configuration remains an optimal way for the generation of quantum correlations in biqudit separable states compared to the cited cases in the text.

5. Conclusion

Two-qubit LQU and LQFI correlations beyond entanglement negativity are studied when a fully separable biqudit state is exposed to the microwave cavity. Certain parameters, such as two-qubit dissipation, coupling, and coherence intensity, characterize the microwave cavity. For the optimal dynamics as well as the generation of LQU and LQFI correlations and entanglement, specific ranges and fixed values of the parameters are provided.

We show that the microwave cavity competes among vital resources for the LQU and LQFI correlations generation in qubit separable states. In the absence of two-qubit dissipation effects, non-classical correlations and entanglement can be generated in the two qubits in a non-Markovian manner. The non-classical correlations and entanglement have been found to exhibit sudden deaths and births at periodic intervals. When the dissipation effects appear, the LQU and LQFI correlations and entanglement emergence in the state depend upon the value of dissipation strength, and both have been found inversely correlated. Interestingly, the coherence intensity of the microwave cavity has been found beneficial for the emergence of non-classical correlations, however, completely restricted the entanglement from generation. This shows the existence and appearance of the LQU and LQFI correlations beyond entanglement in the initial biqudit separable state. Besides, there have been some critical regions of state qubit angle parameter, and SC qubit-cavity coupling strength which should be avoided while some of them should be maintained for a higher degree of non-classical correlations as well as entanglement generation and preservation.

Acknowledgments

The authors are very grateful to the referees for their important remarks which improve the manuscript. This study is supported via funding from the Prince Sattam bin Abdulaziz University project number (PSAU/2023/R/1444).

ORCID

- F. M. Aldosari  <https://orcid.org/0000-0002-0854-9335>
A.-B. A. Mohamed  <https://orcid.org/0000-0001-8761-9583>
A. Rahman  <https://orcid.org/0000-0001-7058-5671>
M. Hashem  <https://orcid.org/0000-0003-0725-0398>

References

1. L. Lami, Non-classical correlations in quantum mechanics and beyond, Doctoral dissertation, Universitat Autònoma de Barcelona (2017).
2. R. Horodecki, P. Horodecki, M. Horodecki and K. Horodecki, *Rev. Mod. Phys.* **81**, 865 (2009).
3. R. V. Mishmash, I. Danshita, C. W. Clark and L. D. Carr, *Phys. Rev. A* **80**, 053612 (2009).
4. L. Ali, M. Ikram, T. Abbas and I. Ahmad, *Quantum Inf. Process.* **21**, 1 (2022).
5. A. K. Ekert and G. M. Palma, *J. Mod. Opt.* **41**, 2413 (1994).
6. D. Song, *Phys. Rev. A* **69**, 034301 (2004).
7. A. Barenco and A. K. Ekert, *J. Mod. Opt.* **42**, 1253 (1995).
8. F. De Martini, F. Sciarrino and C. Vitelli, *Phys. Rev. Lett.* **100**, 253601 (2008).
9. A.-B. A. Mohamed, H. A. Hessian and H. Eleuch, *Optik* **202**, 163500 (2020).
10. T. Q. Data and T. M. Duc, *Optik* **257**, 168744 (2022).
11. H. Ollivier and W. H. Zurek, *Phys. Rev. Lett.* **88**, 017901 (2001).
12. S. Luo, *Phys. Rev. A* **77**, 022301 (2008).
13. S. Luo and S. Fu, *Phys. Rev. Lett.* **106**, 120401 (2011).
14. M.-L. Hu and H. Fan, *New J. Phys.* **17**, 033004 (2015).
15. H. Ollivier and W. H. Zurek, *Phys. Rev. Lett.* **88**, 017901 (2001).
16. B. Dakic, V. Vedral and C. Brukner, *Phys. Rev. Lett.* **105**, 190502 (2010).
17. S. Luo and S. Fu, *Phys. Rev. A* **82**, 034302 (2010).
18. D. Girolami, A. M. Souza, V. Giovannetti, T. Tufarelli, J. G. Filgueiras, R. S. Sarthour, D. O. Soares-Pinto, I. S. Oliveira and G. Adesso, *Phys. Rev. Lett.* **112**, 210401 (2014).
19. H. S. Dhar, M. N. Bera and G. Adesso, *Phys. Rev. A* **991**, 032115 (2015).
20. A. Slaoui, L. Bakmou, M. Daoud and R. A. Laamara, *Phys. Lett. A* **383**, 2241 (2019).
21. S. Elghaayda, M. Y. Abd-Rabbou and M. Mansour, *Mod. Phys. Lett. A* **38**, 2350057 (2023).
22. S. Kim, L. Li, A. Kumar and J. Wu, *Phys. Rev. A* **97**, 032326 (2018).
23. D. Girolami, T. Tufarelli and G. Adesso, *Phys. Rev. Lett.* **110**, 240402 (2013).
24. M. Y. Abd-Rabbou, M. Shamirzaie and S. Khan, *Opt. Quantum Electron.* **55**, 715 (2023).
25. E. P. Wigner and M. M. Yanase, *Proc. Natl. Acad. Sci.* **49**, 910 (1963).
26. A. Wallraff, D. I. Schuster, A. Blais, L. Frunzio, R. S. Huang, J. Majer and R. J. Schoelkopf, *Nature* **431**, 162 (2004).
27. F. Arute, K. Arya, R. Babbush, D. Bacon, J. C. Bardin, R. Barends and J. M. Martinis, *Nature* **574**, 505 (2019).
28. B. Yurke, *J. Opt. Soc. Am. B* **4**, 1551 (1987).
29. J. Q. You and F. Nori, *Phys. Today* **58**, 42 (2005).
30. J. Q. You, C. H. Lam and H. Z. Zheng, *Phys. Rev. B* **63**, 180501 (2001).
31. A. J. Leggett, Diatomic molecules and Cooper pairs, in *Modern Trends in the Theory of Condensed Matter* (Springer, 1980), pp. 13–27.
32. R. I. Shekhter, Y. Galperin, L. Y. Gorelik, A. Isacsson and M. Jonson, *J. Phys.: Condens. Mat.* **15**, R441 (2003).

33. B. S. Palmer, C. A. Sanchez, A. Naik, M. A. Manheimer, J. F. Schneiderman, P. M. Echternach and F. C. Wellstood, *Phys. Rev. B* **76**, 054501 (2007).
34. B. M. Terhal, *Nat. Phys.* **14**, 530 (2018).
35. S. Boixo, S. V. Isakov, V. N. Smelyanskiy, R. Babbush, N. Ding, Z. Jiang and H. Neven, *Nat. Phys.* **14**, 595 (2018).
36. A. Blais, R. S. Huang, A. Wallraff, S. M. Girvin and R. J. Schoelkopf, *Phys. Rev. A* **69**, 062320 (2004).
37. A. U. Rahman, Z. X. Ji and H. G. Zhang, *Eur. Phys. J. Plus* **137**, 1 (2022).
38. A.-B. A. Mohamed and N. Metwally, *Ann. Phys.* **381**, 137 (2017).
39. A. B. Mohamed, H. Eleuch and C. R. Ooi, *Phys. Lett. A* **383**, 125905 (2019).
40. S. Eshete, *Optik* **258**, 168812 (2022).
41. Y. X. Liu, L. F. Wei and F. Nori, *Europhys. Lett.* **67**, 941 (2004).
42. M. Bartkowiak, A. Miranowicz, X. Wang, Y. X. Liu, W. Leoki and F. Nori, *Phys. Rev. A* **83**, 053814 (2011).
43. J. R. Johansson, G. Johansson, C. M. Wilson, P. Delsing and F. Nori, *Phys. Rev. A* **87**, 043804 (2013).
44. Y. J. Zhao, Y. L. Liu, Y. X. Liu and F. Nori, *Phys. Rev. A* **91**, 053820 (2015).
45. H. B. Chen, C. Gneiting, P. Y. Lo, Y. N. Chen and F. Nori, *Phys. Rev. Lett.* **120**, 030403 (2018).
46. C. S. Muoz, A. Lara, J. Puebla and F. Nori, *Phys. Rev. Lett.* **121**, 123604 (2018).
47. H. B. Chen, P. Y. Lo, C. Gneiting, J. Bae, Y. N. Chen and F. Nori, *Nat. Commun.* **10**, 3794 (2019).
48. A. B. Mohamed, A. Rahman, S. M. Younis and N. Zidan, *Opt. Quantum Electron.* **55**, 611 (2023).
49. X. Gu, A. F. Kockum, A. Miranowicz, Y. X. Liu and F. Nori, *Phys. Rep.* **718–719**, 1 (2017).
50. Y.-X. Liu, L. F. Wei and F. Nori, *Phys. Rev. A* **72**, 033818 (2005).
51. S.-X. Wu, J. Zhang, C.-S. Yu and H.-S. Song, *Phys. Lett. A* **378**, 344 (2014).
52. G. Vidal and R. F. Werner, *Phys. Rev. A* **65**, 032314 (2002).
53. S. Ashhab and F. Nori, *Phys. Rev. A* **81**, 042311 (2010).
54. N. Zidan, H. Bakry and A. U. Rahman, *Ann. Phys.* **534**, 2100555 (2022).
55. A. U. Rahman, H. Ali, S. Haddadi and S. M. Zangi, *Alex. Eng. J.* **67**, 425 (2023).
56. Y. N. Guo, M. F. Fang, G. Y. Wang and K. Zeng, *Quantum Inf. Process.* **15**, 5129 (2016).
57. M. Hu and W. Zhou, *Laser Phys. Lett.* **16**, 045201 (2019).